UNDERWATER IMAGE RESTORATION USING ADAPTIVE NEIGHBORHOOD DARK CHANNEL PRIOR

Yu-Chi Pu[1] and Wei-Chang Du[2]

[1]Department of Maritime Information and Technology
National Kaohsiung University of Science and Technology
No. 142, Hai-Chuan Rd., Nanzih Dist., Kaohsiung City 81157, Taiwan
ycpu@nkust.edu.tw

[2]Department of Information Engineering
I-Shou University
No. 1, Sec. 1, Syuecheng Rd., Dashu Dist., Kaohsiung City 84001, Taiwan
wcdu@isu.edu.tw

ABSTRACT. *Dark channel prior (DCP) is the most popular algorithm used in haze removal and underwater image restoration. Nevertheless, a problem that edge regions are blurred, known as halo artifacts, occurs in DCP. In this paper, we propose a novel adaptive neighborhood strategy (AN-DCP) to reduce the halo artifacts in DCP. Our proposed strategy uses the variable size of neighborhood depending on the deviation around the pixel. The large size of the neighborhood helps to select the correct dark pixel in smooth areas, and the small size of the neighborhood helps to preserve the edge characteristics. The experimental results show that this strategy constructs the transmission map more precisely than using the fixed neighborhood size even after the refinement step. The restored scene radiance using the AN-DCP method has fewer halo artifacts near the depth edges than those in DCP. The proposed AN-DCP method ensures improved restoration quality compared with DCP for both hazed and underwater images.*
Keywords: Adaptive neighborhood, Dark channel prior, Halo artifact, Underwater image restoration

1. **Introduction.** Underwater imaging can use various devices, including optical cameras, laser scanners, or sonar devices. Optical and laser images are clear and easily understood, but the distance of the acquisition device from objects is restricted from a few meters to tens of meters. In turbid water, optical vision is effective only at an extremely short distance. Sonar images, which are widely used in undersea exploration, have the advantages of far distance and good penetration. Acoustic sensors capture good distance and size information of objects, but sonar images are corrupted by multiplicative noise. Thus, sonar data are needed for professional interpretation and are unsuitable for short-distance environment exploitation. Some information such as color and texture features can be extracted only from optical images and not from acoustic images.

To effectively detect the underwater state, most underwater vehicles carry high-resolution camera equipment and sonar or laser orientation systems to complement each other. By using fixed surveillance cameras or underwater vehicles equipped with photographic lens, we can obtain real-time underwater images to analyze the characteristics of underwater objects and achieve some specific objectives.

Optical images are rich sources of information. However, in underwater environments, image quality is heavily degraded due to the absorption and scattering effects of light propagation. Dispersion phenomenon refers to the condition in which the object-reflected

light spreads through the water particles, and multiple diffusion caused by the dispersion phenomenon degrades the visibility and contrast of underwater images.

Image restoration is an important preprocessing step for pattern recognition or computer vision such as applications of object detection or recognition. After recovering the quality of a distorted image, the features and information in the image become more obvious to be collected than that without recovering. Therefore, underwater image restoration is an important issue for underwater vision.

Significant research has addressed the technique of underwater image restoration. Schechner and Karpel [1] used a polarizer to reduce degradation effects and obtained clearer images. However, polarization filtering must be conducted when acquiring images so that the method cannot recover existing distortion underwater images. The problem of underwater image restoration is similar to that of haze removal. Some researchers have used the dark channel prior (DCP) strategy to solve the haze removal problem, but a certain degree of distortion still occurs, as in the case of halo artifacts.

In this paper, we propose a novel adaptive neighborhood subdivision strategy based on DCP, and a large number of halo artifacts are removed in the proposed adaptive neighborhood DCP method. The AN-DCP restoration method for underwater or foggy images preserves the silhouette features and reduces the halo artifacts. In the rest of the paper, Section 2 reviews previous work on DCP, Section 3 describes the proposed AN-DCP strategy, Section 4 explores the proposed method and discusses the results, and Section 5 provides the conclusions.

2. **Background.** The scattering and absorption phenomena of the light propagation in underwater environments reduce the visibility of underwater images. The degradation model of underwater images is formulated similar to that of hazed images. The degradation model [2,4] for a hazed or underwater image I at a pixel x can be expressed as

$$I(x) = J(x)t(x) + (1 - t(x))A \tag{1}$$

where $I(x)$ is the observed color vector, $J(x)$ is the scene radiance vector, A is the global atmospheric light (or background light) and $t(x)$ is the medium transmission based on the Beer-Lambert law as follows:

$$t(x) = e^{-\beta d(x)} \tag{2}$$

In (2), β is the attenuation and $d(x)$ is the scene depth.

In recent years, some studies have resolved the underwater image restoration problem by using dehazing algorithms. The most popular methodology is DCP, which was proposed by He et al. [4] for single-image haze removal. The prior comes from natural observation and the statistical result. That is, in the natural scenes, at least one of the RGB color channels is dark around a neighborhood called the dark channel. The formula of the estimated dark channel $J_{dark}(x)$ is as follows and approximately equal to zero:

$$J_{dark}(x) = \min_{c \in \{r,g,b\}} \min_{y \in \Omega(x)} J_c(y) \tag{3}$$

In Equation (3), $J_c(x)$ is a color channel of the scene radiance $J(x)$, and $\Omega(x)$ is the local patch or neighborhood centered at the pixel x. Most researchers use 15×15 as the patch size, as well as 3×3 or 11×11 [4,6-9].

We state the DCP algorithm below shortly. A general dehazing algorithm based on DCP can be divided into the following steps.

Dark channel construction. The size of the local patch $\Omega(x)$ is defined, and then the dark channel value map is obtained by Equation (3).

Atmospheric light estimation. In most haze-opaque regions, the atmospheric light is the scene light. The brightest pixels in the hazy image are considered to be the most

haze-opaque [4]. Thus, the pixel with the brightest dark channel value is used to estimate the atmospheric light.

$$A_c = I_c(\arg \max J_{dark}(x)) \quad \forall c \in \{r, g, b\} \tag{4}$$

However, the brightest value of the dark channel may be a white object in the scene. In practice, the top 0.1% brightest pixels on the dark channel are selected, and are averaged to estimate the atmospheric light.

Transmission map estimation. Using Equations (1), (3), and (4), we can estimate the transmission value $\tilde{t}(x)$ of each pixel as

$$\tilde{t}(x) = 1 - \min_{c \in \{r,g,b\}} \min_{y \in \Omega(x)} \left(\frac{I_c(y)}{A_c} \right) \tag{5}$$

Transmission map refinement. Since the estimated transmission map $\tilde{t}(x)$ in Equation (5) contains certain block effects, it has to be refined according to the original color texture. Many researchers have addressed this issue through methods such as soft matting [4], bilateral filtering [5] and guided filtering [5]. The early refinement proposed by [4] is soft matting, which is time-consuming. Both the bilateral and guided filters are classified as edge-preserving smoothing operators, and the latter has better behavior near the edges than the former. In this study, we use the guided filter to solve the refinement problem. The guided filtering strategy is also faster than the others.

Recovering the scene radiance. From the last step, we obtain the refined transmission map $t(x)$, and then the color channel $J_c(x)$ of the scene radiance $J(x)$ is recovered as follows:

$$J_c(x) = \frac{I_c(x) - A_c}{t(x)} + A_c \quad \forall c \in \{r, g, b\} \tag{6}$$

3. Proposed Method.

3.1. Adaptive neighborhood dark channel prior (AN-DCP).

The DCP method finds the dark channel in a local neighborhood (patch) for each pixel. A dark channel point is the local minimum, and may be covered by several neighbor patches. That is, the dark values are the same in these adjacent patches, and the block effect appears in the dark channel map. The dark channel map is used to estimate the automorphic light and the transmission rate, so the block effect also appears in the transmission map. In most related studies, the patch size for estimating the dark channel is fixed as 15×15 or 11×11 [10].

The decision of the neighborhood size is an important issue. A large neighborhood size increases the probability that a patch contains a dark pixel. By contrast, a small neighborhood may not contain a dark pixel. However, the estimated transmission values are constant in a neighborhood. A large neighborhood size produces the halo artifact near depth edges even after refinement, as shown in Figure 4(c).

In this paper, we adopt the strategy of adjusting the neighborhood size when estimating the medium transmission $\tilde{t}(x)$ in Equation (5) according to the deviation around the pixel. That is, the larger the deviation around the pixel is, the smaller the patch size is.

The decision rule is defined as the Algorithm. The symbol $\Omega_n(x)$ is the neighborhood centered at x with a size of $n \times n$.

The fixed-size neighborhood $\Omega(x)$ in (5) is replaced by the variable-sized neighborhood $\Omega_n(x)$. By adaptively adjusting the neighborhood size, the transmission map is estimated more precisely than using the fixed size. In the rest of the paper, we refer to our method as adaptive neighborhood dark channel prior (AN-DCP).

```
Algorithm GetNeighborhoodSize
Input: the colored image I
Output: NS(x)
Set minSize = 3, maxSize = 15
K(x) ← min   I_c(x)   ∀x ∈ I
      c∈{r,g,b}
compute StdDev_n(x), for n = minSize, minSize+2, ..., maxSize
for each pixel x in image I
    n ← maxSize
    while (StdDev_n(x) > ε and n > minSize) do
        n ← n − 2
    end
    NS(x) ← n
End
```

3.2. **Underwater dark channel prior (UDCP).** In an underwater environment, especially the deep sea, the red channel of the water light is attenuated largely. If the dark channel is computed according to Equation (3), most dark values come from the red channel. Thus, similar to most of the studies on underwater images [9], the dark channel is computed only by considering the green and blue color channels. Thus, Equation (3) is revised as Equation (7). Drews-Jr et al. [10] named the dark channel, excluding the red channel, as UDCP.

$$J_{dark}^{undersea}(x) = \min_{c\in\{g,b\}} \min_{y\in\Omega(x)} J_c(y) \tag{7}$$

In the next section's experiment, the dark channel computation uses either Equation (3) or (7) depending on the image type. However, other details of UDCP are the same as those in traditional DCP implementation.

4. **Experimental Results.** To evaluate the performance of the proposed method, we exploit some experiments using the AN-DCP and DCP methods separately. As we want to verify the effectiveness of the adaptive neighborhood size, the only difference between these two implementations is whether the neighborhood size is variable or fixed. The other steps or parameters are the same.

Figure 1 shows sample images in the experiment. Our method is also appropriate for hazed images, and thus. Figures 1(a) and 1(b) are underwater images and 1(c) and 1(d) are hazed images. However, the dark channel computation uses Equation (7) for underwater images and Equation (3) for hazed images. Figure 2 shows the map of the neighborhood size based on the AN-DCP method. In the experiment, the neighborhood size is set from 3×3 to 15×15 depending on the deviation of the neighborhood. Compared to the original images in Figure 1, the more sophisticated the area is, the finer the neighborhood size in this area is. The depth edges in which the front and back objects are adjacent to each other are subdivided into small neighborhoods. Thus, the more precise transmission rate can be estimated and compared to the one with a fixed neighborhood size.

Figure 3 compares the transmission maps estimated by DCP and AN-DCP. The depth edges in the transmission maps generated by AN-DCP are sharper than those generated by DCP. Figure 3(d) distinguishes the small leaves from the background sky better than Figure 3(b) does. Figure 4 shows the restored scene radiance obtained through these two methods. The halo artifacts near the depth edges are less in the AN-DCP than in the DCP method. Furthermore, a better image can be restored by using the former method than the latter.
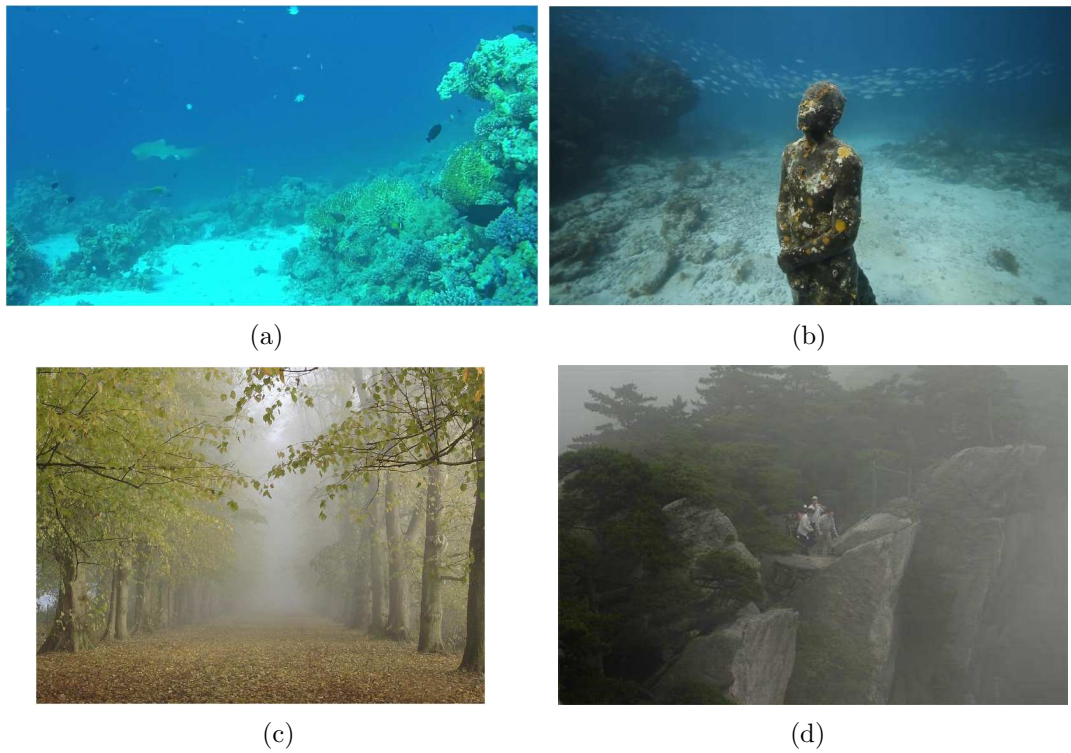
FIGURE 1. Sample images: (a) coral reef [11], (b) sculpture [12] (Courtesy of Jason deCaires Taylor), (c) forest [13], and (d) mountain [13]
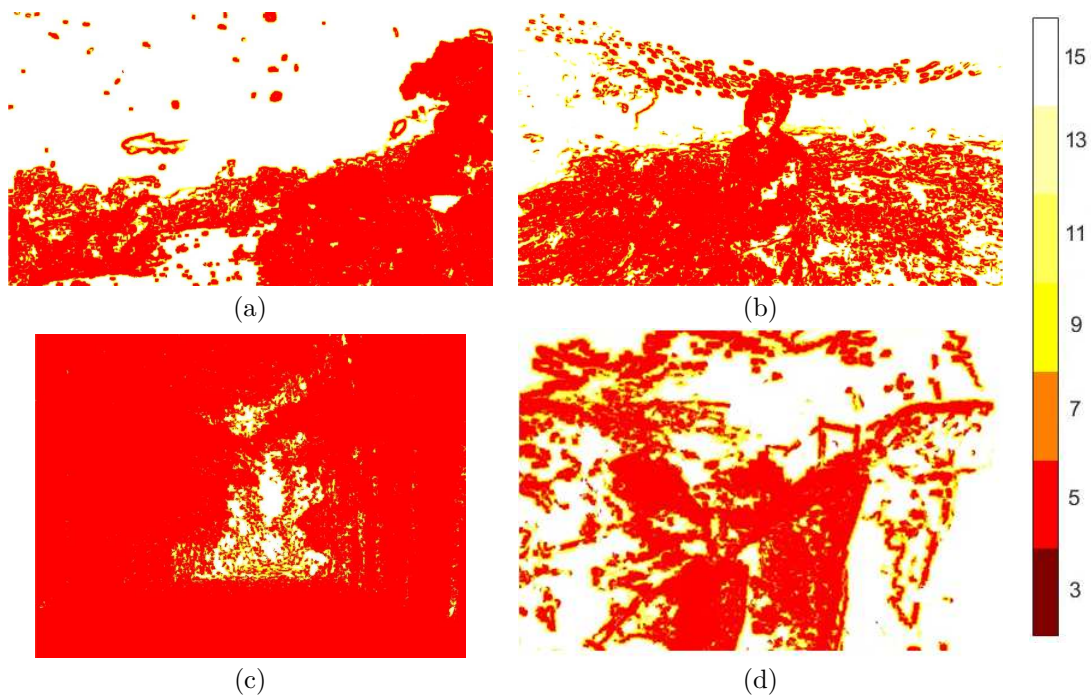

FIGURE 2. (color online) The maps of the neighborhood size using AN-UDCP or AN-DCP for the images in Figure 1. The color value of the pixel represents the neighborhood size around the pixel.
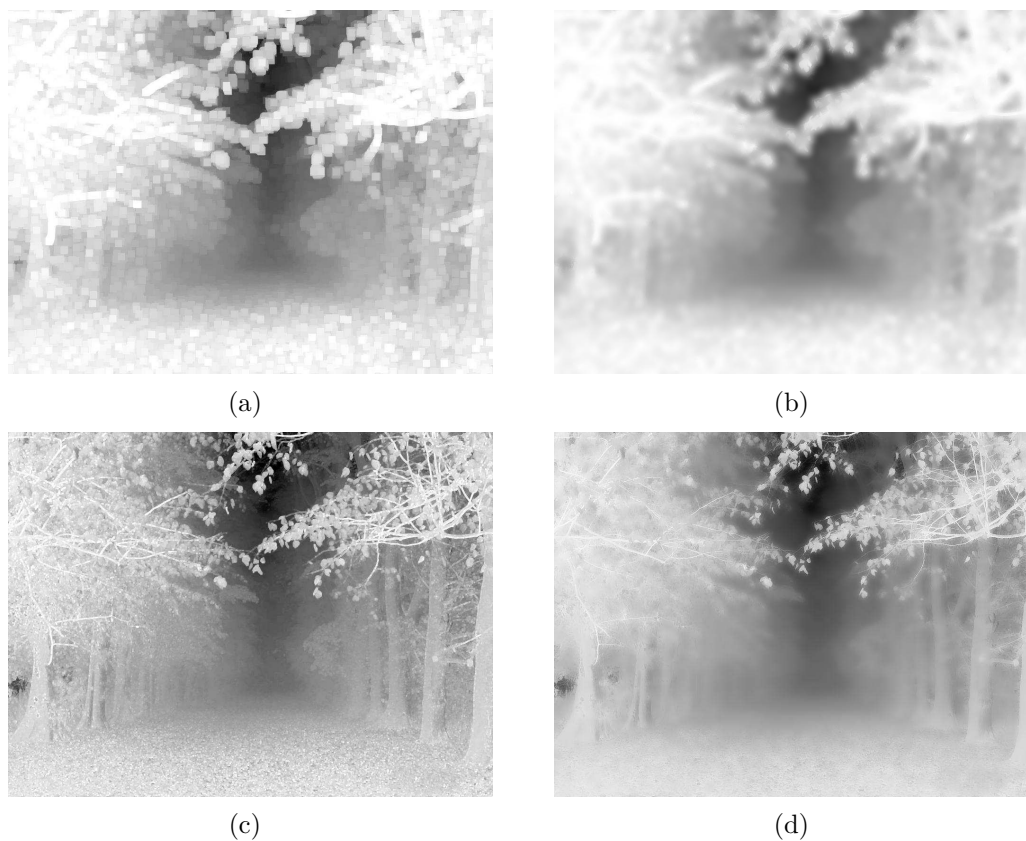
FIGURE 3. Transmission map comparison for the image in Figure 1(c): (a) fixed neighborhood size (DCP), (b) refined transmission map of (a), (c) variable neighborhood size (AN-DCP), and (d) refined transmission map of (c)
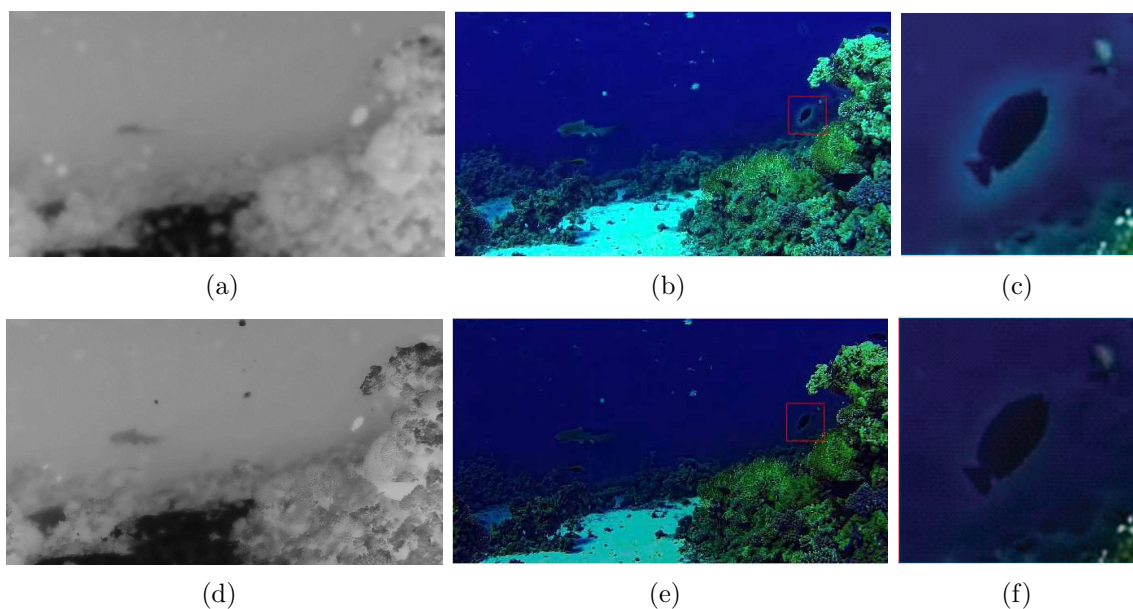

FIGURE 4. Comparison of transmission maps and restored scene radiance for the image in Figure 1(a): (a) refined transmission map using UDCP, (b) restored scene radiance using UDCP, (c) enlarging the red rectangle in (a), (d) refined transmission map using AN-UDCP, (e) restored scene radiance using AN-UDCP, and (f) enlarging the red rectangle in (e)

5. **Conclusions.** In this paper, we propose a novel adaptive neighborhood selection (AN-DCP) when estimating the transmission map. The experimental results show that this strategy constructs the transmission map more precisely than the original fixed neighborhood even after the refinement step. The restored scene radiance has fewer halo artifacts than the original one caused by the coarse patch size.

For simplicity, other phenomena causing the underwater image degradation are ignored in this study, such as color shift phenomenon, which is due to the different attenuation rates of lights as a result of varying wavelengths. Moreover, in the deep sea, even though the blue light is attenuated, artificial light is necessary but it also degrades underwater images because of the glare. These issues will be investigated in future research to deal with a larger variety of distorted underwater images.

REFERENCES

[1] Y. Y. Schechner and N. Karpel, Recovery of underwater visibility and structure by polarization analysis, *IEEE Journal of Oceanic Engineering*, vol.30, no.3, pp.570-587, 2005.

[2] H. Koschmieder, Theorie der horizontalen sichtweite, *Beitrage zur Physik der freien Atmosphare*, vol.12, pp.171-181, 1924.

[3] R. Fattal, Single image dehazing, *ACM Trans. Graphics (TOG)*, vol.27, no.3, 2008.

[4] K. He, J. Sun and X. Tang, Single image haze removal using dark channel prior, *Proc. of IEEE Conf. Computer Vision and Pattern Recognition*, 2009.

[5] C. Tomasi and R. Manduchi, Bilateral filtering for gray and color images, *Proc. of the 6th IEEE Int'l Conf. Computer Vision*, p.839, 1998.

[6] K. He, J. Sun and X. Tang, Guided image filtering, *IEEE Trans. Pattern Anal. Mach. Intell.*, vol.35, pp.1397-1409, 2013.

[7] J. Y. Chiang and Y. C. Chen, Underwater image enhancement by wavelength compensation and dehazing, *IEEE Trans. Image Processing*, vol.21, no.4, pp.1756-1769, 2012.

[8] N. Carlevaris-Bianco, A. Mohan and R. M. Eustice, Initial results in underwater single image dehazing, *Oceans*, pp.1-8, 2010.

[9] A. Galdran, D. Pardo, A. Picón and A. Alvarez-Gila, Automatic red-channel underwater image restoration, *Journal of Visual Communication and Image Representation*, vol.26, pp.132-145, 2015.

[10] P. Drews-Jr, E. R. Nascimento, S. Botelho and M. Campos, Underwater depth estimation and image restoration based on single images, *IEEE Computer Graphics and Applications*, vol.36, no.2, pp.24-35, 2016.

[11] Sharm el Sheikh - Dive - Februar 2014, *YouTube*, https://youtu.be/BzsBtjoGWSA, 2017.

[12] Jason deCaires Taylor and Museo Subaquatico de Arte, *YouTube*, https://youtu.be/oip5M3IJ4bI, 2017.

[13] K. He, *Single Image Haze Removal*, http://kaiminghe.com/cvpr09/index.html, 2017.